Highly active methanol decomposition catalyst derived from Pd-hydrotalcite dispersed on mesoporous silica

Yanyong Liu [a,*], Kunio Suzuki [b], Satoshi Hamakawa [b], Takashi Hayakawa [b,*], Kazuhisa Murata [b], Tomoko Ishii [a] and Mikio Kumagai [a]

[a] *Chemical Technology Division, Institute of Research and Innovation, Takada 1201, Kashiwa, Chiba 277, Japan*
[b] *National Institute of Materials and Chemical Research, Tsukuba Research Center, AIST, Higashi 1-1, Tsukuba, Ibaraki 305, Japan*

Received 29 January 2000; accepted 21 April 2000

Pd-hydrotalcite (abbreviated as Pd(HT)) was dispersed on HMS (hexagonal mesoporous silica) by synthesizing Pd(HT) in an HMS suspension, and the resultant product (Pd(HT)/HMS) was used as a catalyst precursor for methanol decomposition to synthesis gas. The IR spectra of Pd(HT)/HMS showed all the bands of Pd(HT) and HMS with little shift, which indicated that Pd(HT) was synthesized in the Pd(HT)/HMS. Pd(HT)/HMS did not show the XRD pattern of Pd(HT) when the mass ratio of Pd(HT) to HMS was from 2/1 to 1/2. This indicated that Pd(HT) was formed in very small particles in the Pd(HT)/HMS after dispersion. Two endothermic peaks of Pd(HT) in the DTA curve shifted to lower temperatures in the Pd(HT)/HMS because the small Pd(HT) particles formed in the Pd(HT)/HMS were easily collapsed by heat treatment. Pd(HT)/HMS was thermally decomposed and reduced to form a supported Pd catalyst (abbreviated Pd(Mg(Al)O)/HMS) for methanol decomposition. Pd(Mg(Al)O)/HMS at 3.6 wt% showed a 52.5% conversion which was much higher than those over 3.6 wt% Pd(Mg(Al)O) (34.7%) and 3.6 wt% Pd/HMS (13.7%) for methanol decomposition at 523 K. The conversions of methanol over Pd(Mg(Al)O) and Pd/HMS increased with the increase in Pd loadings from 3.6 to 15 wt% and decreased when the Pd loadings were over 15 wt%. In contrast, the conversion over Pd(Mg(Al)O)/HMS increased with the increase in Pd loading even when the Pd loading was up to 30%. 30 wt% Pd(Mg(Al)O)/HMS showed a 91.7% conversion which was about twice that over 15 wt% Pd(Mg(Al)O) (47.1%) at 523 K. The Pd(Mg(Al)O)/HMS catalyst showed a larger BET surface area and Pd metal surface area than those of Pd(Mg(Al)O). By characterization using XPS analyses, the metal–support interaction between small Pd and small Mg(Al)O became stronger in the Pd(Mg(Al)O)/HMS catalyst. Large surface area, high Pd dispersion and strong metal–support interaction caused the high catalytic activity for methanol decomposition to synthesis gas over the Pd(Mg(Al)O)/HMS catalyst.

Keywords: palladium, hydrotalcite, mesoporous silica, methanol decomposition, synthesis gas

1. Introduction

The decomposition of methanol to synthesis gas has received growing attention recently because the reaction possesses several practical applicable possibilities, such as in fuel cells and for on-board reforming for vehicles [1]. We are focusing on the methanol decomposition reaction because it is endothermic and the reversible reaction can operate in a suitable temperature range. It can transform waste heat energy from industrial locations or power plants using methanol decomposition and transport the chemical energy to remote areas such as residential areas [2]. The equilibrium conversion of methanol decomposition reaches around 100% under atmospheric pressure at 473 K.

$$CH_3OH \rightleftharpoons CO + 2H_2 \quad \Delta H = 22 \text{ kcal mol}^{-1} \qquad (1)$$

Cu-, Ni- and Pd-based catalysts are known to be active for methanol decomposition to CO and H_2. For Cu-based catalysts, Ba, Si and Mn oxides promote the activity and Cr oxides improve the stability, but Cu-based catalysts still suffer from slow deactivation and methyl formate (MF) is usually observed as a by-product [3]. In the case of Ni-based catalysts, the selectivity for synthesis gas usually is not sufficient due to the formation of methane [4]. For recovery of waste heat from industries by methanol decomposition, the catalyst must be active and selective at low temperature. The Pd-based catalysts seem to be preferred, and the activity is largely affected by the supports. ZrO_2 and CeO_2 have been reported to be effective supports for Pd in the reaction [5,6]. Hydrotalcite ($Mg_3Al(OH)_{16}CO_3{\cdot}4H_2O$, denoted by HT) has brucite-like positively charged layers of magnesium and aluminum octahedra-sharing edges and has interstitial carbonate anions to compensate for the charges [7]. Calcined hydrotalcite (Mg(Al)O) is a peculiar support for Pt and Pd catalysts for several reactions [8,9]. We had reported that Pd(Mg(Al)O) showed high activity and selectivity for methanol decomposition [10].

The recent synthesis of silica-based mesoporous materials, such as M41S [11], HMS [12] and FSM-16 [13], by the cooperative assembly of periodic inorganic and surfactant-based structures has attracted great interest because it extends the range of molecular-sieve materials into the very large pore regime. High thermal stability (up to 1198 K), larger surface area (above 1000 $m^2\,g^{-1}$), uniform-sized pores and adsorption capacity for aromatic organic molecules render these materials very interesting for catalysis and support [14–16]. In the present study, in order to maximize the surface area and increase the Pd dispersion of

* To whom correspondence should be addressed.

the catalyst, we dispersed Pd(HT) on HMS by synthesizing Pd(HT) in the HMS suspension. The novel catalyst which was derived from HMS-supported Pd(HT) showed high activity and selectivity for synthesis gas from methanol decomposition.

2. Experimental

2.1. Synthesis

Pd(HT) was prepared by a coprecipitation method at pH 10.0, by adding an aqueous solution containing $Pd(NO_3)_2$, $Mg(NO_3)_2$ and $Al(NO_3)_3$ (molar ratio Mg to Al is 3/1) to a solution containing a slight excess of Na_2CO_3 at 333 K. A 2 mol dm^{-3} NaOH aqueous solution was added during the operation to maintain the pH value 10. The resultant precipitate was washed and dried at 373 K for 24 h. The Pd(Mg(Al)O) catalyst was obtained by calcination of the Pd(HT) at 698 K for 3 h.

HMS was prepared by adding a clear solution of $Si(OC_2H_5)_4$ (1.00 mol) in ethanol (6.54 mol) to a stirring solution of dodecylamine (0.27 mol) and HCl (0.02 mol) in water (36.3 mol) [12]. Allowing the resulting gel to age for 18 h at ambient temperature afforded the crystalline templated product. The sample was dried at 373 K and calcined in air at 923 K for 4 h to remove the structurally incorporated template. Pd/HMS was prepared by an impregnation method.

Pd(HT)/HMS was prepared as follows. HMS powders ($<$100 mesh) were added to an aqueous solution containing $Pd(NO_3)_2$, $Mg(NO_3)_2$ and $Al(NO_3)_3$, and then stirred vigorously for 30 min at 333 K to form a suspension. A solution of Na_2CO_3 was acidified by adding dilute HNO_3 to reach pH 10. The suspension was slowly added to the Na_2CO_3 solution at 333 K under vigorous stirring. The operation was completed in about 1 h keeping the pH at 10 by adding 2 mol dm^{-3} NaOH. After aging at 363 K for 1 h, the precipitate was filtered off, washed with distilled water, and finally dried at 373 K for 24 h. The molar ratio Mg to Al was 3, and the mass ratio Pd(HT) to HMS was 1/2 or 2/1 in the Pd(HT)/HMS precursor. The Pd(Mg(Al)O)/HMS catalyst was obtained by calcination of the Pd(HT)/HMS precursor at 698 K for 3 h. A mixed catalyst, Pd(Mg(Al)O) + HMS, was prepared as a reference for the Pd(Mg(Al)O)/HMS catalyst by stirring the Pd(HT) suspension and HMS suspension together for 30 min at 333 K, then filtering off the solid and calcining at 698 K for 3 h. The designed Pd loadings were 3.6, 15 and 30 wt% for the catalysts, and the actual amounts of Pd loadings in the catalysts were measured by ICP analysis.

2.2. Instrumentation

Fourier transform infrared (FTIR) spectroscopy was recorded by a JASCO FT/IR-7000 spectrometer using KBr pellets over the range of 400–4000 cm^{-1} under atmospheric conditions. Powder X-ray diffraction (XRD) patterns were measured using a MAC Science MXP-18 diffractometer with Cu Kα radiation operated at 40 kV and 50 mA. Thermogravimetric and differential thermal analyses (TG-DTA) were carried out using a Shimadzu TGA-50 instrument. The sample was heated under an atmosphere of flowing N_2 at a heating rate of 5 K min^{-1} from room temperature to 1073 K. N_2 adsorption isotherms were measured at 77 K using a Belsorp 28SA automatic adsorption instrument. The samples were dried at 573 K for 8 h before the measurement. The surface area was obtained from a BET (Brunauer–Emmett–Teller) plot, and the pore size distribution was performed by the BJH (Barrett–Joyner–Halenda) method. Inductively coupled plasma (ICP) analyses were carried out using a Thermo Jarrell Ash IRIS/AP. The Pd metal surface area and Pd particle sizes were measured by the CO pulse adsorption method at room temperature [17]. 20 mg of the catalyst reduced in 100 ml min^{-1} of H_2 flow at 673 K for 20 min was used for the measurements. Transmission electron micrograph (TEM) analyses were carried out using a Jeol JEM-2010/EDS system. The *ex situ* treated samples were supported on carbon-coated copper grids for the experiment. X-ray photoelectron (XPS) spectra were collected at a chamber pressure of $\sim 10^{-9}$ Torr (1 Torr $= 1.33 \times 10^{-4}$ MPa) using a Phi-5500 ESCA spectrometer employing Mg Kα radiation (1253.6 eV). The binding energy of Pd was calibrated using C_{1s} of 284.6 eV.

2.3. Catalytic reaction

The catalytic test was conducted using a fixed-bed flow reactor under atmospheric pressure from 423 to 573 K. A 300 mg catalyst (70 mesh) body was sandwiched between quartz wool and packed in a 10 mm $\varnothing$ U-shaped quartz tubular reactor. The top of the thermocouple was contacted with the catalyst surface to determine the reaction temperature. After reduction in a flow of 10% H_2 at 673 K for 1 h, the reaction was started under a flow of 40% methanol diluted with N_2 gas at a total flow rate of 10 000 ml h^{-1} g$_{cat}^{-1}$. The products were analyzed by three on-line TCD gas chromatographs. Molecular sieve 5A was used for CO and H_2 analyses with He and Ar as the carrier gas, respectively. For the analyses of methanol, methyl formate (MF), dimethyl ether (DME) and CO_2, Porapak Q was used with He as the carrier gases. The selectivity of each product was calculated based on the converted methanol.

3. Results and discussion

3.1. Characterization of the Pd(HT)/HMS precursor

Infrared spectroscopic features of the framework vibrations of Pd(HT), calcined HMS and Pd(HT)/HMS are shown in figure 1. For HMS, the peak at 1090 cm^{-1} and

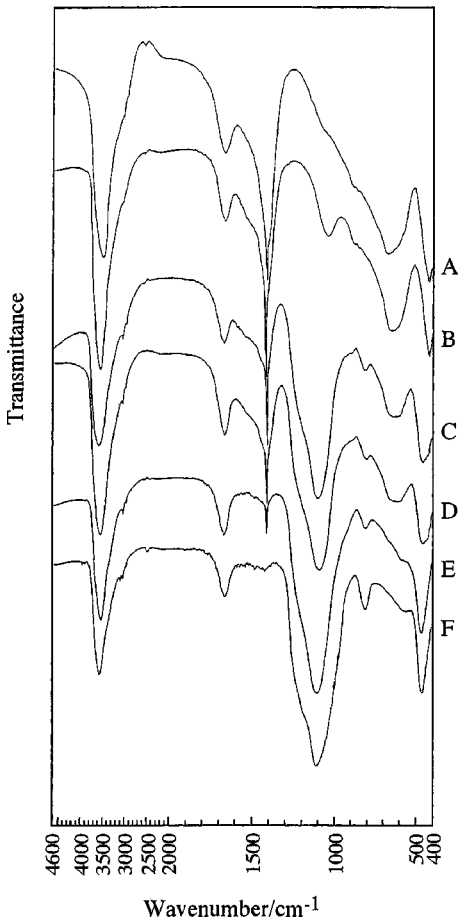

Figure 1. The FTIR spectra of (A) 3.6 wt% Pd(HT), (B) 3.6 wt% Pd(HT)/HMS (mass ratio Pd(HT) to HMS = 10/1), (C) 3.6 wt% Pd(HT)/HMS (mass ratio 2/1), (D) 3.6 wt% Pd(HT)/HMS (mass ratio 1/2), (E) 3.6 wt% Pd(HT)/HMS (mass ratio 1/10) and (F) HMS.

its shoulders may be assigned to the asymmetric stretching of Si–O–Si [18]. The peaks at 470 and 810 cm^{-1} are also given by the "internal" bands of SiO_4 tetrahedra and the broad band at 3400 cm^{-1} associated with hydrogen-bonded silanol group vibration [19]. Weak peaks are observed at 1400–1500 cm^{-1} from aliphatic C–H bending and at 2800–3100 cm^{-1} from aliphatic C–H stretching vibrations, which indicated that the template was not completely removed for HMS after calcination at 923 K for 4 h. As for Pd(HT), the peaks at 1380 cm^{-1} ($\gamma 3$), 820 cm^{-1} ($\gamma 2$) and 630 cm^{-1} ($\gamma 4$) are associated with CO_3^{2-} vibrations between the layers, and the peaks at 410 and 430 cm^{-1} are related to the cation–oxygen vibrations in the brucite-like layer [7]. The peak at 1645 cm^{-1} may be assigned to the water-bending band between layers. The synthesized Pd(HT)/HMS showed all the peaks of HMS and Pd(HT) with little shift, which indicated that Pd(HT) had been synthesized in the Pd(HT)/HMS precursor.

The X-ray diffraction patterns of Pd(HT), calcined HMS and Pd(HT)/HMS are shown in figure 2. Calcined HMS exhibited a strong reflection (100) at about 2.3° corresponding to $d = 4$ nm. Hexagonal order weaker (110) and (200) reflections were also observed in the 2θ range from 4.0° to

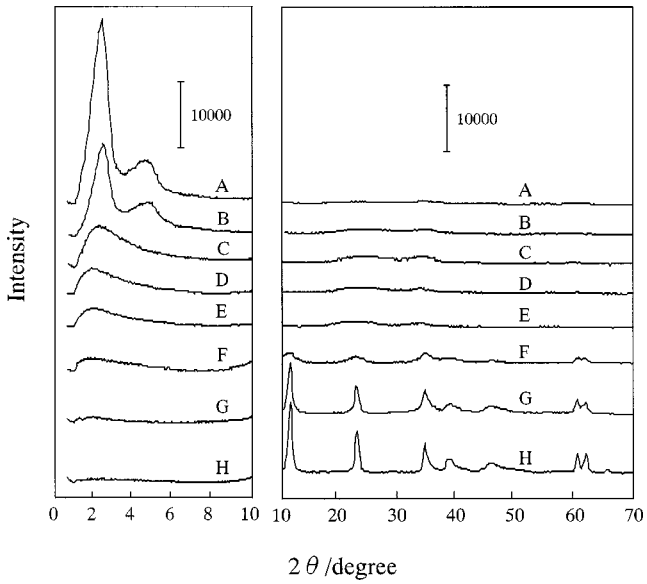

Figure 2. The XRD patterns of (A) HMS, (B) 3.6 wt% Pd/HMS, (C) 3.6 wt% Pd(HT)/HMS (mass ratio Pd(HT) to HMS = 1/10), (D) 3.6 wt% Pd(HT)/HMS (mass ratio 1/2), (E) 3.6 wt% Pd(HT)/HMS (mass ratio 2/1), (F) 3.6 wt% Pd(HT)/HMS (mass ratio 10/1), (G) 3.6 wt% Pd(HT) and (H) HT ($Mg_6Al_2(OH)_{16}CO_3{\cdot}4H_2O$).

6.0°. Pd(HT) showed the pattern of a layered structure from 10° to 70° ($d(003) = 0.771$ nm, $d(110) = 0.155$ nm). Pd(HT)/HMS showed the XRD pattern of Pd(HT) when the mass ratio Pd(HT) to HMS was 10/1, but the intensity decreased greatly. No peak was observed in the XRD pattern of Pd(HT)/HMS from 10° to 70° when the mass ratio Pd(HT) to HMS was from 2/1 to 1/2. We think that the Pd(HT) particles, which formed on the surface and/or in the pores of HMS in the Pd(HT)/HMS, are too small to exhibit an XRD pattern. The intensity of the XRD pattern from 1° to 10° decreased with the increase in the mass ratio of Pd(HT) in the Pd(HT)/HMS. The pores of HMS blocked by the formed Pd(HT), or by the walls of HMS being partly destroyed, caused the decrease in the reflections at low 2θ in the XRD pattern of Pd(HT)/HMS.

Figure 3 shows the TG and DTA curves of Pd(HT), calcined HMS, and Pd(HT)/HMS. Because HMS had been calcined at 923 K for 4 h, there is almost no weight loss in the TG curve. The DTA curve of HMS can be regarded as the base line of the instrument. Two weight loss stages were observed for Pd(HT) in the TG curve, coinciding with two endothermic peaks in the DTA profiles. The first weight loss below 473 K was ascribed to the loss of physically absorbed and interlayer water. The second weight loss in the temperature range from 573 to 698 K could be attributed to removal of CO_2 from the interlayer carbonate anions and hydroxy groups from the brucite-like layers [7]. Pd(HT)/HMS also shows two endothermic peaks in the DTA and two weight losses in TD due to the loss of absorbed and interlayer water during the first stage and the loss of carbonate anions and hydroxy groups during the second stage. The two peaks in the DTA curve of Pd(HT)/HMS shifted to low temperatures coinciding with

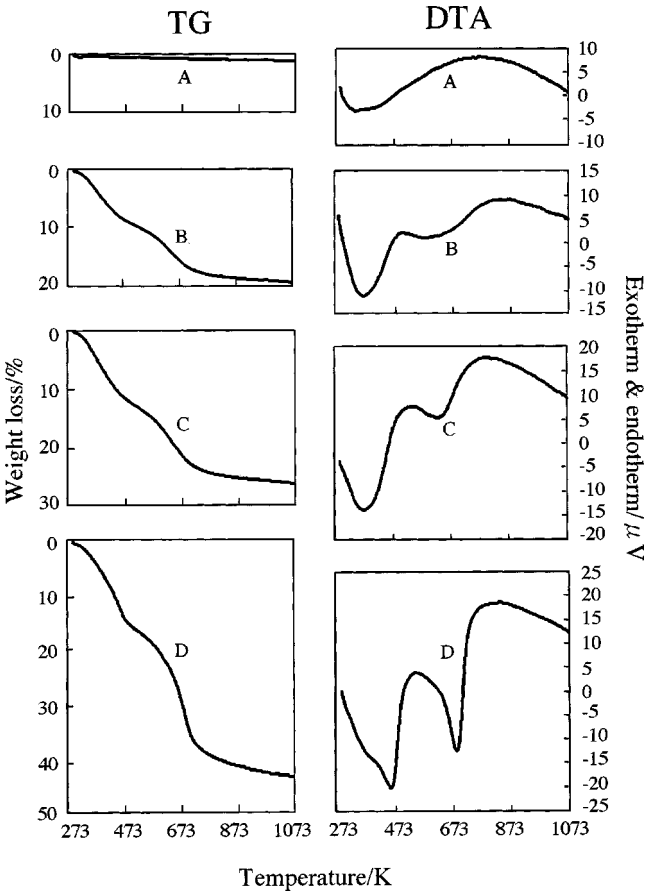

Figure 3. Thermogravimetric and differential thermal analyses of (A) HMS, (B) 3.6 wt% Pd(HT)/HMS (mass ratio Pd(HT) to HMS = 1/2), (C) 3.6 wt% Pd(HT)/HMS (mass ratio 2/1) and (D) 3.6 wt% Pd(HT).

the weight losses in the TG curve. This indicated that the Pd(HT) particles formed in Pd(HT)/HMS were very small and collapsed at low temperature. TG and DTA analyses also confirmed that there is no impurity in the samples.

3.2. Catalytic activity for methanol decomposition

The effect of the ratio of Pd(Mg(Al)O) to HMS in Pd(Mg(Al)O)/HMS catalysts is shown in figure 4. Both at 473 and 523 K, the maximum conversions were obtained when the mass ratio Pd(HT) to HMS was 1/2 in the Pd(HT)/HMS precursor for the 3.6 wt% Pd(Mg(Al)O)/HMS catalyst. However, the mass ratio of 2/1 between Pd(HT) and HMS in the Pd(HT)/HMS precursor was used for 15 and 30 wt% Pd(Mg(Al)O)/HMS to ensure sufficient amounts of Mg(Al)O in the catalysts.

The conversion and product distribution for various catalysts with 3.6 wt% Pd loading are shown in table 1. All of the Pd-containing catalysts prepared in this work showed high selectivities for CO and H_2. Very small amounts of methane, carbon dioxide, methyl formate, dimethyl ether and water formed as by-products. The 3.6 wt% Pd/HMS catalyst, which has the highest surface area, showed a low conversion of 13.7% at 523 K. This result indicated that HMS is not a suitable support for methanol decomposition,

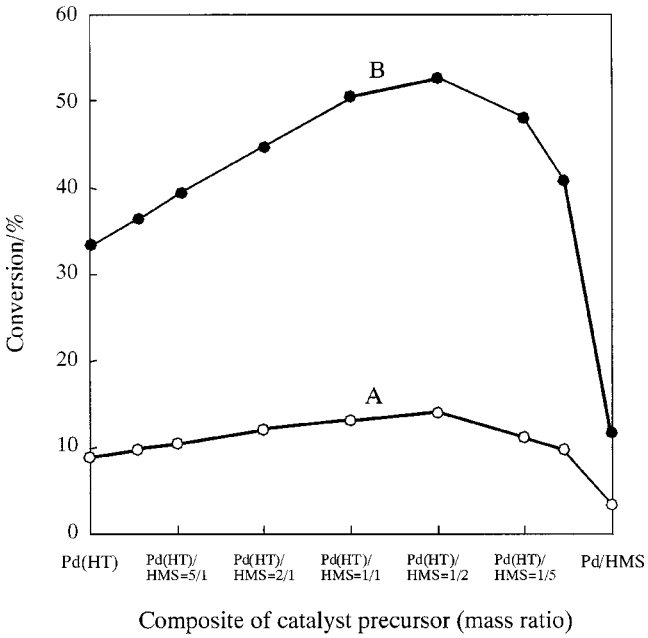

Figure 4. Catalytic activity of 3.6 wt% Pd supported catalysts derived from various precursors. Reaction temperature: (A) 473 and (B) 523 K.

although Pd/SiO_2 is one of the most active catalysts for methanol synthesis from CO and H_2 [20]. Pd(Mg(Al)O) is an efficient catalyst for methanol decomposition [10] and showed 34.7% of conversion with 3.6 wt% Pd loading at 523 K. The Pd(Mg(Al)O)/HMS catalyst with 3.6 wt% Pd showed a 52.5% conversion which was much higher than that over the 3.6 wt% Pd(Mg(Al)O) catalyst at 523 K. This proved that the dispersion of Pd(Mg(Al)O) on HMS increased the catalytic activity for methanol decomposition. The mixed 3.6 wt% Pd(Mg(Al)O) + HMS catalyst showed a 33.6% conversion which was much less than that over 3.6 wt% Pd(Mg(Al)O)/HMS catalyst at 523 K, which indicated that the uniform dispersion of Pd(HT) on HMS was very important for improving the catalytic activity for methanol decomposition.

The effect of Pd loading dependence on various catalysts is shown in table 2. The methanol conversion over Pd(Mg(Al)O) and Pd/HMS increased with the increase in the Pd loadings from 3.6 to 15 wt% but decreased when the loading of Pd was over 15 wt%. However, the conversion over Pd(Mg(Al)O)/HMS increased with the increase in the Pd loading even when the Pd loading was up to 30 wt%. 30 wt% Pd(Mg(Al)O)/HMS showed a 91.7% conversion which was about twice that over 15 wt% Pd(Mg(Al)O) (47.1%) at 523 K.

The rates of methanol decomposition over the various supported Pd catalysts were plotted against the reaction temperature from 423 to 573 K in figure 5. The apparent activation energies calculated from the data in figure 5 were 59.8, 56.4 and 52.4 kJ mol^{-1} for the 3.6 wt% Pd/HMS, 3.6 wt% Pd(Mg(Al)O) and 3.6 wt% Pd(Mg(Al)O)/HMS. Pd(Mg(Al)O)/HMS at 3.6 wt% Pd showed the lowest activation energy among the catalysts.

Table 1
Catalytic activity and product distribution over various catalysts.[a]

Catalyst[b]	Reaction temp. (K)	Conv. MeOH (%)	Selectivity (%)					
			CO	CO_2	CH_4	DME	MF	H_2
Pd(Mg(Al)O)/HMS[c]	473	14.7	96.6	3.3	0	0	0.1	89.2
	523	52.5	99.8	0	0	0.2	0	98.2
	573	96.5	99.4	0	0.4	0.3	0	99.1
Pd/HMS	473	3.2	98.9	0	0	0	1.1	94.9
	523	13.7	99.9	0	0	0	0.1	98.4
	573	45.4	99.5	0	0.5	0	0	99.1
Pd(Mg(Al)O)	473	9.2	98.4	0.4	0	0.6	0.4	96.5
	523	34.7	99.6	0	0	0.3	0.1	99.3
	573	88.6	99.5	0	0.3	0.2	0	99.2
Pd(Mg(Al)O) + HMS[c]	473	8.5	99.3	0.5	0	0.3	0	97.0
	523	33.6	99.7	0	0	0.3	0	99.2
	573	87.2	99.6	0	0	0.4	0	99.3

[a] $F/W = 10\,000$ ml h^{-1} g_{cat}^{-1}, CH_3OH 40%, N_2 60%.
[b] Pd loading 3.6 wt%.
[c] Mass ratio Pd(HT) to HMS = 1/2.

Table 2
Activity and selectivity for methanol decomposition over the catalysts with various Pd loading.[a]

Catalyst	Pd loading (wt%)	Conv. MeOH (%)	Selectivity (%)					
			CO	CH_4	CO_2	DME	MF	H_2
Pd(Mg(Al)O)	3.6	34.7	99.6	0	0	0.3	0.1	99.3
	15	47.1	99.2	0	0	0.5	0.3	99.2
	30	43.2	98.7	0.6	0.1	0.2	0.4	98.8
Pd/HMS	3.6	13.7	99.9	0	0	0	0.1	98.4
	15	25.6	99.4	0	0.1	0.3	0.2	99.1
	30	20.8	99.0	0	0	0.8	0.2	98.6
Pd(Mg(Al)O)/HMS[b]	3.6	45.1	99.7	0	0	0.2	0.1	99.1
	15	78.4	99.8	0	0	0.1	0.1	99.7
	30	91.7	98.5	1.0	0	0.3	0.2	97.8

[a] Reaction temperature 523 K, $F/W = 10\,000$ ml h^{-1} g_{cat}^{-1}, CH_3OH 40%, N_2 60%.
[b] Mass ratio Pd(HT) to HMS = 2/1.

3.3. Characterization of Pd(Mg(Al)O)/HMS catalyst

Figure 6 presents the N_2 adsorption–desorption isotherms and figure 7 shows the pore size distribution curves by BJH analysis [21] for HMS, 3.6 wt% Pd/HMS, 3.6 wt% Pd(Mg(Al)O) and 3.6 wt% Pd(Mg(Al)O)/HMS. All samples showed the isotherms of type IV according to BDDT classification [22]. The hysteresis loop was close to the H1 type for HMS according to IUPAC classification [23]. The abrupt step in the $P/P_0 = 0.25$–0.35 region and the corresponding maximum in the pore distribution curve indicated the existence of uniform mesopores in the size range of 2.6–2.8 nm. The N_2 adsorption–desorption isotherm of 3.6 wt% Pd/HMS was similar to that of HMS and showed a pore distribution at about 2.8 nm. The pore distribution was relatively sharp but the BET surface area decreased due to the loading of Pd for 3.6 wt% Pd/HMS. Pd(Mg(Al)O) at 3.6 wt% Pd showed a hysteresis loop close to the H2 type [23] and the pore system was very poor. Pd(Mg(Al)O)/HMS at 3.6 wt% Pd showed H3 type hysteresis loops [23]. The same wt% Pd(Mg(Al)O)/HMS showed pore size distributions at about 2.8 nm, but the pore system was greatly reduced compared to HMS and 3.6 wt%

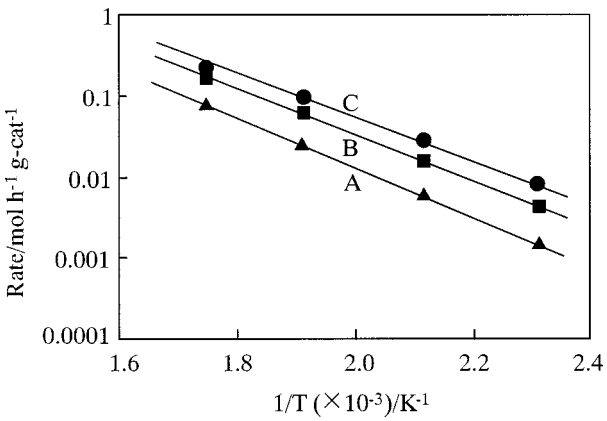

Figure 5. Arrhenius plot of rate of methanol decomposition over various catalysts: (A) 3.6 wt% Pd/HMS, (B) 3.6 wt% Pd(Mg(Al)O) and (C) 3.6 wt% Pd(Mg(Al)O)/HMS (mass ratio Pd(HT) to HMS = 1/2).

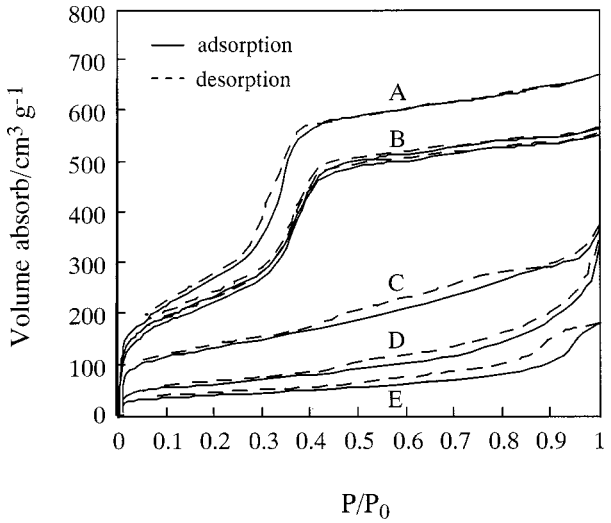

Figure 6. N_2 adsorption/desorption isotherms of (A) HMS, (B) 3.6 wt% Pd/HMS, (C) 3.6 wt% Pd(Mg(Al)O)/HMS (mass ratio Pd(HT) to HMS = 1/2), (D) 3.6 wt% Pd(Mg(Al)O)/HMS (mass ratio Pd(HT) to HMS = 2/1) and (E) 3.6 wt% Pd(Mg(Al)O).

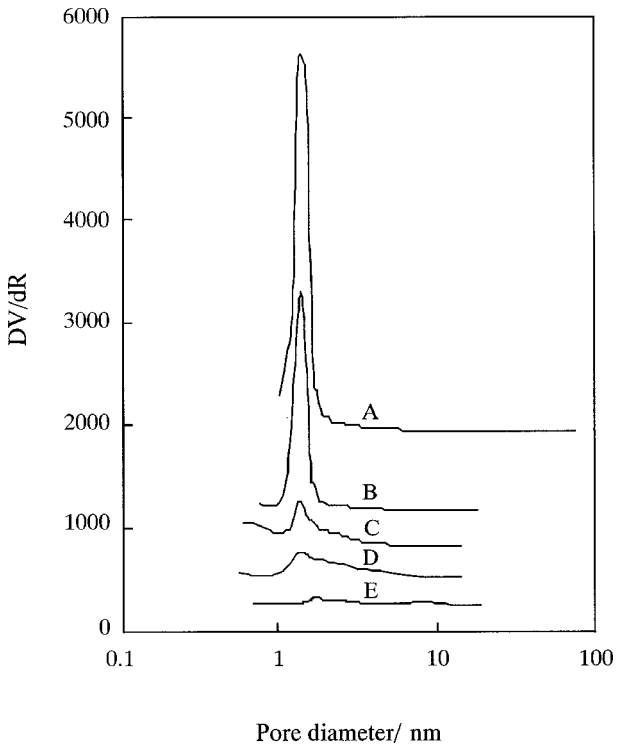

Figure 7. Pore size distributions of (A) HMS, (B) 3.6 wt% Pd/HMS, (C) 3.6 wt% Pd(Mg(Al)O)/HMS (mass ratio Pd(HT) to HMS = 1/2), (D) 3.6 wt% Pd(Mg(Al)O)/HMS (mass ratio Pd(HT) to HMS = 2/1) and (E) 3.6 wt% Pd(Mg(Al)O).

Pd/HMS, which was due to blocking of the HMS pores by Pd(Mg(Al)O) for 3.6 wt% Pd(Mg(Al)O)/HMS.

Physical properties of Pd/HMS, Pd(Mg(Al)O) and Pd(Mg(Al)O)/HMS catalysts are shown in table 3. CO adsorption by a pulse method was used to measure the Pd metal surface area, and the Pd particle sizes were calculated from the Pd metal surface area [17]. Pd(Mg(Al)O)/HMS showed a much larger BET surface area than that of Pd(Mg(Al)O) and showed a larger Pd metal surface area than those of Pd(Mg(Al)O) and Pd/HMS with the same Pd loading, which leads to the high catalytic activity for methanol decomposition over Pd(Mg(Al)O)/HMS. The relatively small Pd particles were obtained even at high Pd loading for the Pd(Mg(Al)O)/HMS catalyst. Thus the conversion of methanol decomposition increased with the increase in the Pd loading even when the Pd loading was up to 30 wt% over the Pd(Mg(Al)O)/HMS catalyst.

Table 3
Physical properties of the catalysts containing palladium.

Catalyst	Pd loading[a] (wt%)	Surface area ($m^2\ g_{cat}^{-1}$) BET	Surface area ($m^2\ g_{cat}^{-1}$) Pd metal[b]	Particle size of Pd[b] (nm)
Pd/HMS	3.6 (3.5)	818	4.4	3.3
	15 (15.2)	684	9.9	6.4
	30 (29.1)	513	9.6	12.7
Pd(Mg(Al)O)	3.6 (3.3)	143	3.7	3.7
	15 (14.6)	112	11.2	5.4
	30 (27.3)	87	12.0	9.6
Pd(Mg(Al)O)/HMS	3.6 (3.4)[c]	361	4.7	3.0
	3.6 (3.3)[d]	332	4.5	3.1
	15 (14.1)[d]	296	16.2	3.6
	30 (26.4)[d]	234	19.0	5.8

[a] The values in parentheses were obtained by ICP and were used to calculate Pd metal surface area and Pd particle size.
[b] Pd metal surface and Pd particle size were measured by CO pulse method.
[c] Mass ratio Pd(HT) to HMS = 1/2.
[d] Mass ratio Pd(HT) to HMS = 2/1.

TEM images for 3.6 wt% Pd/HMS, 3.6 wt% Pd (Mg(Al)O) and 3.6 wt% Pd(Mg(Al)O)/HMS catalysts are shown in figure 8. The average Pd particle sizes of the catalysts were in agreement with the results of the CO measurement (table 3). For 3.6 wt% Pd/HMS, HMS displayed the diffraction pattern of a hexagonal structure (figure 8(a)) [12], and the Pd particle size was about 3 nm (figure 8(b)). 3.6 wt% Pd(Mg(Al)O) (figure 8(c) before reaction, figure 8(d) after reaction) showed a Pd particle size (figure 8(c)) similar to that of 3.6 wt% Pd/HMS, though the BET surface area of Mg(Al)O was much lower than that of HMS. This is due to the strong metal–support interaction between the noble metal and Mg(Al)O [8]. Figure 8 (e) and (f) shows TEM images of 3.6 wt% Pd(Mg(Al)O)/HMS before and after reaction. It was confirmed that Pd particles were located on the Mg(Al)O in the 3.6 wt% Pd(Mg(Al)O)/HMS catalyst. The particle sizes did not increase after reaction for Pd(Mg(Al)O) [10] and Pd(Mg(Al)O)/HMS catalysts (figure 8 (d) and (f)).

Surface analyses of the Pd catalysts were carried out using XPS analyses (figure 9). The peak position of Pd for 3.6 wt% Pd(Mg(Al)O) was discernibly higher than that for metallic palladium (Pd^0 $3d_{5/2}$ 334.9 eV, Pd^0 $3d_{3/2}$ 340.2 eV [24]), which showed that Pd in Pd(Mg(Al)O) had a partly positive charge. This result proved the existence of a strong interaction between Pd and Mg(Al)O support in Pd(Mg(Al)O). The Pd XPS peak of Pd(Mg(Al)O)/HMS

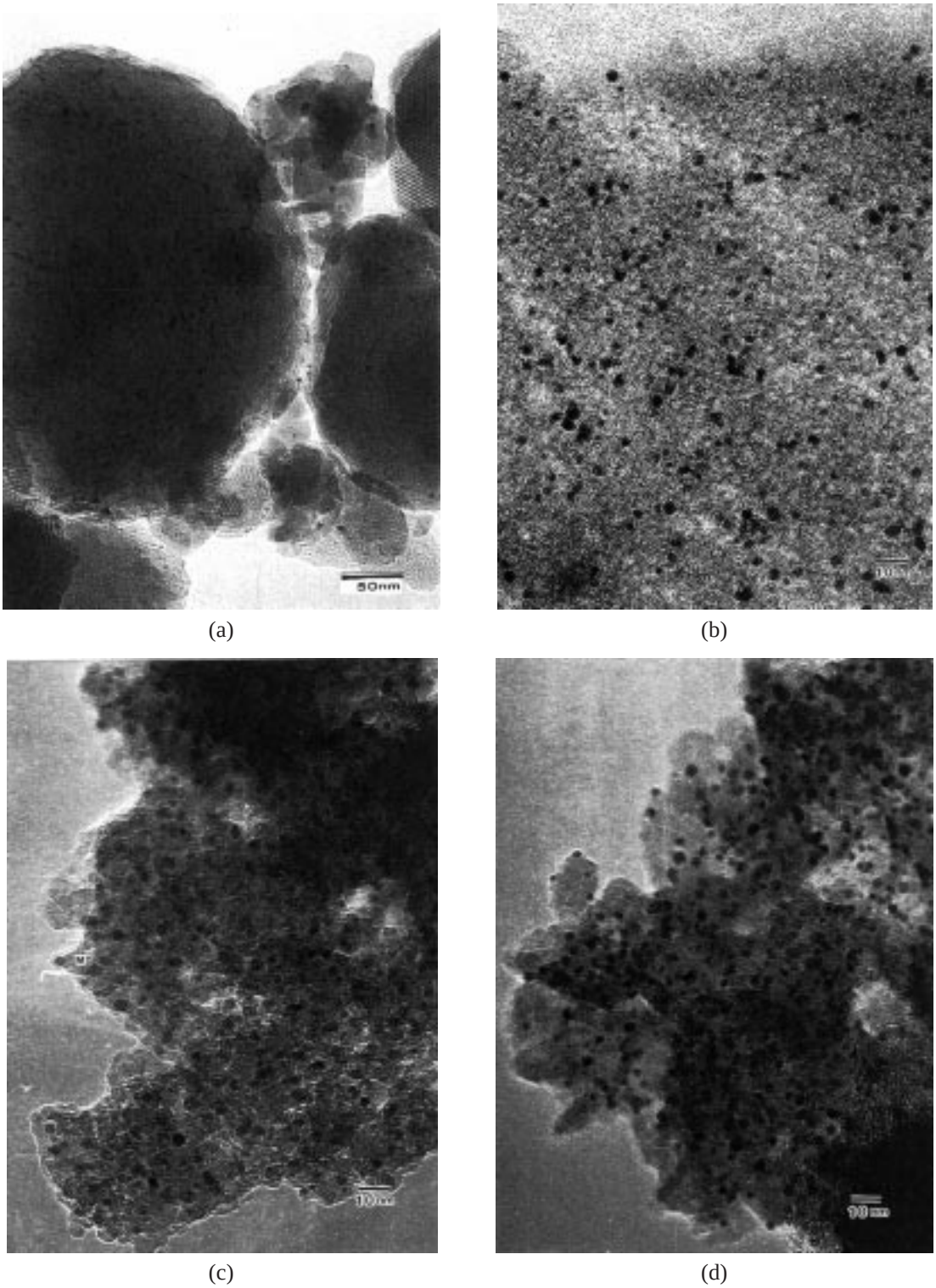

Figure 8. Transmission electron micrographs of (a) 3.6 wt% Pd/HMS (before reaction), (b) 3.6 wt% Pd/HMS (before reaction), (c) 3.6 wt% Pd(Mg(Al)O) (before reaction), (d) 3.6 wt% Pd(Mg(Al)O) (after reaction), (e) 3.6 wt% Pd(Mg(Al)O)/HMS (mass ratio Pd(HT) to HMS = 1/2) (before reaction) and (f) 3.6 wt% Pd(Mg(Al)O)/HMS (mass ratio Pd(HT) to HMS = 1/2) (after reaction).

also shifted to positive and even showed a higher value than that of Pd(Mg(Al)O). The metal–support interaction became stronger due to the small Mg(Al)O particles and the small Pd particles in the Pd(Mg(Al)O)/HMS catalyst.

3.4. Side reactions and reaction mechanism

Over all the Pd-containing catalysts tested, the selectivities for CO were larger than 96% (table 1). The by-products were methane, carbon dioxide, methyl formate, dimethyl

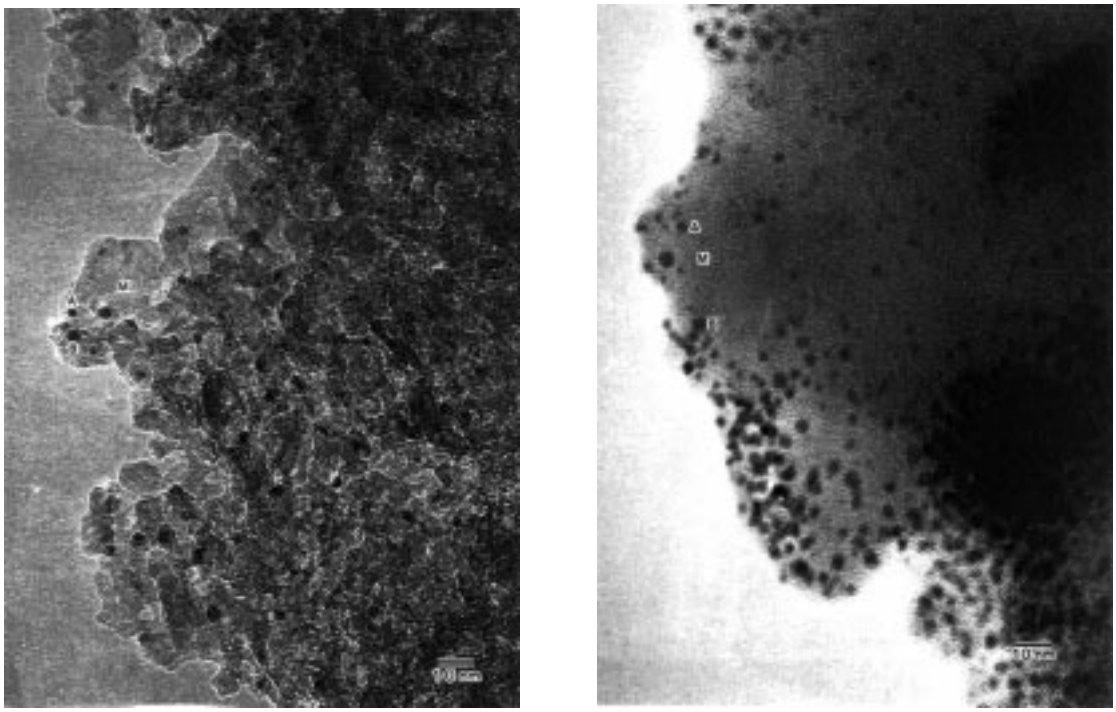

(e) (f)

Figure 8. (Continued.)

ether and water. They might be considered to be produced by the following side reactions [25]:

$$2CH_3OH \rightleftharpoons (CH_3)_2O + H_2O \text{ (dehydration)} \quad (2)$$
$$2CH_3OH \rightleftharpoons HCO_2CH_3 + 2H_2 \text{ (dehydrogenation)} \quad (3)$$
$$CO + 3H_2 \rightleftharpoons CH_4 + H_2O \text{ (methanation)} \quad (4)$$
$$CO + H_2O \rightleftharpoons CO_2 + H_2 \text{ (water–gas shift)} \quad (5)$$
$$CH_3OH + H_2O \rightleftharpoons 3H_2 + CO_2 \text{ (steam reforming)} \quad (6)$$
$$2CO \rightleftharpoons C + CO_2 \text{ (Boudart)} \quad (7)$$

Methyl formate which is usually detected as a main by-product over copper-containing catalysts was formed due to dehydrogenation (equation (3)), and methane which is usually detected as a main by-product over Ni-containing catalysts was formed due to methanation (equation (4)). Carbon dioxide was most likely the result of equations (5)–(7). Carbon formed in equation (7) causes the deactivation of the catalysts [26].

Methanol decomposition was considered to occur successively according to the following equations [27]:

$$CH_3OH(g) \rightleftharpoons CH_3O(a) + H(a) \quad (8)$$
$$CH_3O(a) + H(a) \rightleftharpoons CH_2O(a) + H_2(g) \quad (9)$$
$$CH_2O(a) \rightleftharpoons CHO(a) + H(a) \quad (10)$$
$$CHO(a) \rightleftharpoons CO(a) + H(a) \quad (11)$$
$$CO(a) \rightleftharpoons CO(g) \quad (12)$$
$$2H(a) \rightleftharpoons H_2(g) \quad (13)$$

The dissociation of the hydroxyl group by equation (8) is rapid on the noble metals. The abstraction of the C–H bond in the absorbed methoxy group CH_3O (equation (9)) is a rate-determining step [27]. When Pd assumes a partly oxidized state in the catalyst, an electron is withdrawn from the methoxy group to Pd and the C–H bond of the methoxy

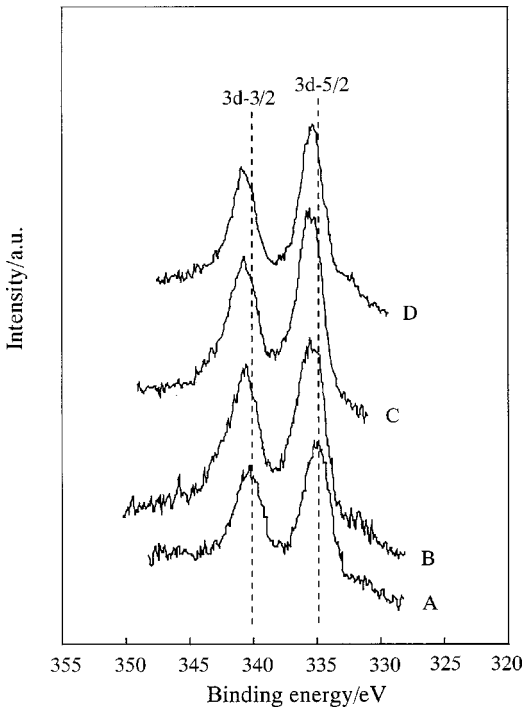

Figure 9. X-ray photoelectron spectra of Pd 3d for supported Pd catalysts: (A) 3.6 wt% Pd/HMS, (B) 3.6 wt% Pd(Mg(Al)O), (C) 3.6 wt% Pd(Mg(Al)O)/HMS (mass ratio Pd(HT) to HMS = 1/2) (before reaction), (D) 3.6 wt% Pd(Mg(Al)O)/HMS (mass ratio Pd(HT) to HMS = 1/2) (after reaction).

group will be weakened, resulting in the acceleration of the reaction. It is reported that the partly oxidized Pd is more active than zero-valent Pd for either methanol decomposition to synthesis gas [28] or methanol synthesis from synthesis gas [29]. We also observed that the binding energy of Pd increased in the order of Pd/HMS, Pd(Mg(Al)O) and Pd(Mg(Al)O)/HMS in the XPS spectra (figure 9) correlated with the activity order for methanol decomposition. This suggests that the metal–support interaction between Pd and Mg(Al)O increased by dispersion of Pd(Mg(Al)O) on HMS and improved the catalytic activity for methanol decomposition.

4. Conclusions

Pd(HT) was dispersed on HMS by synthesizing Pd(HT) in an HMS suspension. IR spectra confirmed that Pd(HT) was synthesized in Pd(HT)/HMS. XRD patterns and TG-DTA analyses indicated that Pd(HT) was formed in very small particles in the Pd(HT)/HMS.

Pd(Mg(Al)O)/HMS showed much higher conversions than those over Pd(Mg(Al)O) and Pd/HMS with the same Pd loading. The methanol conversion over Pd(Mg(Al)O) and Pd/HMS increased with the increase in Pd loading from 3.6 to 15 wt% and decreased when the Pd loading was over 15 wt%, but the conversion over Pd(Mg(Al)O)/HMS increased even when the Pd loading was up to 30 wt%.

Pd(Mg(Al)O)/HMS showed a larger BET surface area and a larger Pd metal surface area than those of Pd (Mg(Al)O) with the same Pd loading. Moreover, the Pd binding energy in XPS spectra increased after dispersion of Pd(HT) on HMS, which indicated that the metal–support interaction became stronger between the small particles of the Mg(Al)O support and the Pd particles in Pd(Mg(Al)O)/HMS catalysts. These are the reasons why Pd(Mg(Al)O)/HMS showed high activity for methanol decomposition. High surface area and strong metal–support interaction caused relatively small Pd particles to be obtained even at high Pd loading for the Pd(Mg(Al)O)/HMS catalyst, which caused the conversion of methanol decomposition to increase with the increase in the Pd loading even when the Pd loading was up to 30 wt% over the Pd(Mg(Al)O)/HMS catalyst.

Acknowledgement

YL, TI and MK gratefully acknowledge the financial support from the New Energy and Industrial Technology Development Organization.

References

[1] W.H. Cheng, Acc. Chem. Res. 32 (1999) 685.
[2] Y. Matsumura, K. Kagawa, Y. Usami, M. Kawazoe, H. Sakurai and M. Haruta, J. Chem. Soc. Chem. Commun. (1997) 657.
[3] W.H. Cheng, C.Y. Shiau, T.H. Liu, H.L. Tung, J.F. Lu and C.C. Hsu, Appl. Catal. A 170 (1998) 215.
[4] M. Suehiro, Y. Nagaki, T. Inui and Y. Takegami, J. Jpn. Petrol. Inst. 26 (1983) 150.
[5] Y. Matsumura, M. Okumura, Y. Usami, K. Kagawa, H. Yamashita, M. Anpo and M. Haruta, Catal. Lett. 44 (1997) 189.
[6] Y. Usami, K. Kagawa, M. Kawazoe, Y. Matsumura, H. Sakurai and M. Haruta, Stud. Surf. Sci. Catal. 118 (1998) 83.
[7] F. Cavani, F. Trifirò and A. Vaccari, Catal. Today 11 (1990) 173.
[8] R.J. Davis and E.G. Derouane, Nature 349 (1991) 313.
[9] S. Narayanan and K. Krishna, J. Chem. Soc. Chem. Commun. (1997) 1991.
[10] R. Shiozaki, T. Hayakawa, Y. Liu, T. Ishii, M. Kumagai, S. Hamakawa, K. Suzuki, T. Itoh, T. Shishido and K. Takehira, Catal. Lett. 58 (1999) 131.
[11] C.T. Kresge, M.E. Leonowicz, W.J. Roth, J.C. Vartuli and J.C. Beck, Nature 359 (1992) 710.
[12] P.T. Tanev, M. Chibwe and T.J. Pinnavaia, Nature 368 (1994) 321.
[13] S. Inagaki, Y. Fukushima and K. Kuroda, J. Chem. Soc. Chem. Commun. (1993) 680.
[14] A. Sayari, Chem. Mater. 8 (1996) 1840.
[15] C.A. Koh, R. Nooney and S. Tahir, Catal. Lett. 47 (1997) 199.
[16] I.V. Kozhevnikov, A. Sinnema, R.J.J. Jansem, K. Pamin and H. van Bekkum, Catal. Lett. 30 (1995) 241.
[17] J. Sarkany and R.D. Gonzalez, J. Catal. 76 (1982) 75.
[18] K.I. Kamitsos, A.P. Patsis and G. Kordas, Phys. Rev. B 48 (1993) 12499.
[19] E.M. Flanigen, H. Khatami and H.A. Szymanski, Adv. Chem. Ser. 101 (1997) 201.
[20] E.P. Barrett, L.G. Joyner and P.H. Halenda, J. Am. Chem. Soc. 73 (1951) 373.
[21] S.H. Ali and J.G. Goodwin, Jr., J. Catal. 171 (1997) 333.
[22] S.J. Gregg and K.S.W. Sing, in: *Adsorption, Surface Area and Porosity* (Academic Press, London, 1991).
[23] K.S.W. Sing, D.H. Everett, R.A.W. Haul, L. Moscou, R.A. Pierotti, J. Rouquerol and T. Siemieniewska, Pure Appl. Chem. 57 (1985) 603.
[24] L.E. Davis, N.C. MacDonald, P.W. Palmberg, G.E. Riach and R.E. Weber, in: *Handbook of X-Ray Photoelectron Spectroscopy* (Physical Electronics Industries, 1976).
[25] A.D. Schmitz, D.P. Eyman and K.B. Gloer, Energy Fuels 8 (1994) 729.
[26] H. Niiyama, S. Tamai, J.S. Kim and E. Echigoya, J. Jpn. Petrol. Inst. 24 (1981) 322.
[27] D.W. Mckee, Trans. Faraday Soc. 64 (1968) 2200.
[28] Y. Usami, K. Kagawa, M. Kawazoe, Y. Matsumura, H. Sakurai and M. Haruta, Appl. Catal. A 171 (1998) 123.
[29] J.M. Driessen, E.K. Poels, J.P. Hindermann and V. Ponec, J. Catal. 82 (1983) 26.